MAGNETIC RESONANCE IN MEDICINE 23, 179–192 (1992)

Diffusion Imaging of the Human Brain *in Vivo* Using High-Speed STEAM MRI

KLAUS-DIETMAR MERBOLDT, WOLFGANG HÄNICKE, HARALD BRUHN, MICHAEL L. GYNGELL, AND JENS FRAHM

Max-Planck-Institut für biophysikalische Chemie, Postfach 2841, D-3400 Göttingen, Federal Republic of Germany

Received August 10, 1990; revised October 2, 1990

This paper describes a new method for diffusion imaging of the human brain *in vivo* that is based on a combination of diffusion-encoding gradients with high-speed STEAM MR imaging. The single-shot sequence 90°-TE/2–90°-TM–$(\alpha$-TE/2–STE$)_n$ generates n = 32–64 differently phase-encoded stimulated echoes STE yielding image acquisition times of 576 ms for a 48 × 128 data matrix. Diffusion encoding is performed during the first TE/2-interval as well as during each readout period. Phantom studies reveal a quantitative agreement of calculated diffusion coefficients with literature values. EKG triggering completely eliminates motion artifacts from diffusion-weighted single-shot STEAM images of human brain *in vivo*. While signal attenuation of the cerebrospinal fluid (CSF) is predominantly due to flow, that observed for gray and white matter results from diffusion. Evaluated diffusion coefficients yield $(1.0 \pm 0.1) \times 10^{-5}$ cm^2 s^{-1} for gray matter, $(0.5 \pm 0.1) \times 10^{-5}$ cm^2 s^{-1} for white matter with the diffusion encoding parallel to the main orientation of the myelin sheath of the neurofibrils, and $(0.3 \pm 0.1) \times 10^{-5}$ cm^2 s^{-1} for white matter and a perpendicular orientation. All studies were performed at 2.0 T using a conventional 10 mT m^{-1} gradient system.

INTRODUCTION

The nondestructive determination of the molecular self-diffusion coefficient by NMR (*1*) provides direct access to a physical parameter that is related to fundamental structural and dynamic properties of the system under investigation. Unfortunately, techniques for diffusion measurements fail when extended in a simplistic way to *in vivo* applications. Major difficulties arise from the presence of patient movements, breathing, brain pulsations, macroscopic fluid flow, and microcirculation (perfusion) (*2*). Thus, the evaluation of meaningful diffusion coefficients becomes severely compromised.

Several approaches have been proposed that overcome various problems associated with bulk motion in the presence of the strong diffusion gradients. Among these are motion-rephasing gradient waveforms (*3*), which minimize signal losses caused by "in-scan" motions, EKG triggering, which synchronizes *periodic* "scan-to-scan" motions, and averaging of sequentially recorded images (*4–7*), which reduces image artifacts due to incoherent motions. Most promising, however, are recent attempts that combine diffusion measurements with snapshot echo-planar imaging (EPI) (*8*). Unfortunately, EPI techniques require major hardware modifications and further suffer from a strong sensitivity to susceptibility differences.

0740-3194/92 $3.00

This paper describes a new high-speed diffusion MRI technique based on the single-shot STEAM (*st*imulated *e*cho *a*cquisition *m*ode) imaging sequence (*9*), which has been recently applied for single cardiac cycle imaging of the human heart (*10*). Although the diffusion-weighted version of the high-speed STEAM sequence does not require a special gradient system, its performance as well as range of applicabilities would benefit from the availability of stronger gradient strengths and/or shorter switching times. In contrast to conventional diffusion-weighted STEAM MRI sequences (*11*), high-speed STEAM imaging is effectively performed within a few hundreds of milliseconds. With the use of long diffusion times the overall measuring time may be about 1 s.

METHODOLOGICAL ASPECTS

High-Speed STEAM Imaging

Figure 1 shows a schematic RF pulse and gradient sequence for high-speed diffusion imaging using stimulated echoes. The two leading 90° RF pulses (1.024 ms, Gaussian shape) prepare a pool of longitudinal magnetization that is attenuated by T_1 relaxation during a middle interval TM. This magnetization is read out as a series of STE signals by the application of n low flip angle pulses (0.64 ms, Gaussian shape, α = 8–16°) using a "repetition time" of a few milliseconds (box in Fig. 1). The bandwidths of the RF pulses and the corresponding slice selection gradient strengths are adjusted so that the 90° pulses excite twice the slice thickness determined by the low flip angle read pulses. The reason for this is that the sequential application of three Gaussian-

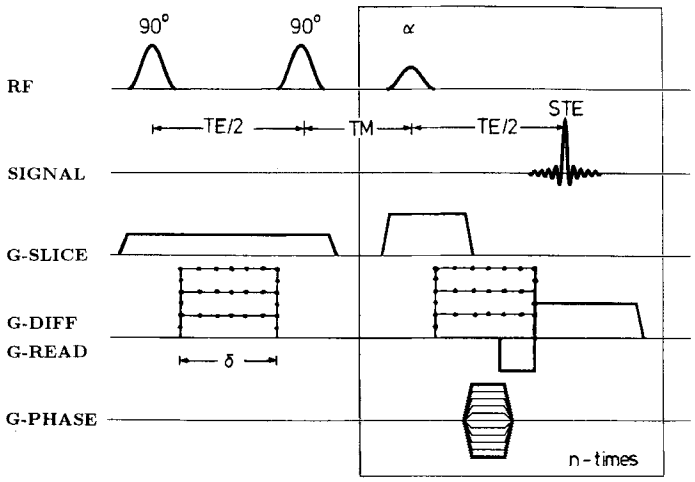

FIG. 1. Schematic RF pulse and gradient sequence for high-speed diffusion imaging using stimulated echoes (STEAM). Single-shot imaging is accomplished by reading the longitudinal magnetization prepared by the two slice-selective 90° RF pulses (outside the box) by a series of slice-selective low flip angle pulses (inside the box) that excite n differently phase-encoded STE signals. For diffusion weighting self-compensating gradient pulses are applied within the first TE/2-interval and during each individual readout period. In general, diffusion gradients may be switched in one, two, or all three gradient axes.

shaped RF pulses with identical slice thickness considerably reduces the effective slice thickness.

For single-shot imaging the individual STE signals are differently phase-encoded as in conventional Fourier imaging. Measuring times of fractions of a second are achieved by reducing the spatial resolution to data matrices of 32–64 × 128 pixels. Depending on the number of phase-encoding steps the flip angle may be optimized to use most of the available longitudinal magnetization. It should be noted that magnetization recovery during the scan does not "refill" the pool of the initially prepared longitudinal magnetization. Instead, the low flip angle read pulses excite recovered magnetization in the form of a free induction decay signal that becomes automatically dephased by magnetic field gradient switches before acquisition of the STE signal.

In contrast to fast scan techniques such as FLASH and EPI that are based on gradient-recalled echo signals, high-speed STEAM sequences acquire the data as an RF refocused STE signal with the echo time TE being determined by the separation of the first two RF pulses (TE/2). The physical properties of the sequence therefore resemble the features of conventional spin-echo images. In particular, STEAM images do not suffer from chemical shift artifacts or signal losses due to tissue susceptibility differences. Moreover, flow signals are eliminated from the images, a feature most advantageously exploited in high-speed cardiac MRI (*10*).

Diffusion-Weighted High-Speed STEAM Imaging

In diffusion-weighted high-speed STEAM MRI gradient pulses are incorporated into the sequence in such a way that the dephasing effect of the first gradient in the initial TE/2-interval is compensated by a corresponding rephasing gradient pulse in each readout interval (G-DIFF, dotted lines in Fig. 1). The duration of the diffusion gradients is restricted to a few milliseconds, here δ = 8.9 ms, to keep the repetition time of the readout interval and the corresponding imaging time as short as possible. Nevertheless, the diffusion weighting (as well as the T_1 attenuation) of each individual STE signal is slightly different due to an increase of the diffusion time with increasing number of the repetition cycles. Since the time scale for diffusion processes is given by the separation of the diffusion gradient pulses, an *effective* diffusion time for a high-speed STEAM image may be deduced from the middle interval and the time required to reach the zero phase-encoding gradient step that predominantly determines image contrasts. In the present study the actual imaging process required 576 ms for the acquisition of 48 Fourier lines with a repetition time of 12 ms. By using an asymmetric coverage of *k*-space with 20 Fourier lines or 240 ms before and 28 Fourier lines or 336 ms after zero phase encoding the effective diffusion time was set to Δ = 1000 ms (TM = 760 ms) for most applications. This value represents a compromise between the imposed diffusion weighting that must be sufficiently strong for reliable evaluations, and a good signal-to-noise ratio (SNR) for components with short T_1 relaxation times. In fact, although the maximum difference in the diffusion weighting of low and high spatial frequencies is of the order of 30% for Δ = 1000 ms, quantitative evaluations of diffusion coefficients were not affected.

A data matrix of 48 × 128 pixels was chosen because larger matrices resulted in long measuring times, whereas smaller matrices suffered from unacceptably poor spatial

resolution. Of course, shorter imaging times as well as much shorter diffusion times may be achieved by the use of stronger gradient strengths. For example, an increase by a factor of two in gradient power transforms into an approximately fourfold reduction of the diffusion time and a significant improvement in the SNR of the diffusion-weighted images. Furthermore, investigations of restricted diffusion are facilitated by extending the range of accessible diffusion times.

It should be emphasized that even for the strongest diffusion gradients no image artifacts due to brain motion were observed in single-shot STEAM images for acquisitions with an EKG-trigger delay of 200–400 ms after the R wave (heart rate 60–70). Other delays resulted in visible ghosting artifacts in the phase-encoding dimension of the images probably reflecting the presence of coherent movements due to brain pulsations. Further experimental observations supporting the negligible influence of macroscopic motions onto the diffusion-weighted STEAM images result from the purely linear signal attenuation observed as a function of the square of the gradient strength. The observed differences in diffusion coefficients for gray and white matter by a factor of two in directly neighboring ROIs would also be difficult to understand if the signal attenuation is significantly affected or even dominated by motion. Moreover, the quantitative evaluations are in general agreement with recent results from diffusion-weighted EPI studies (see below).

Diffusion measurements on phantoms and healthy human volunteers were performed at 2.0 T using a Siemens Magnetom whole-body system equipped with a conventional gradient system providing 10 mT m^{-1} per axis. Diffusion gradient pulses were either switched simultaneously in two directions to increase the available gradient power or in different directions in sequential applications for the investigation of anisotropy effects. Informed consent was obtained prior to the investigations.

Calculations of Self-Diffusion Coefficients

Molecular self-diffusion coefficients may be represented in diffusion maps that are calculated from a series of images with different diffusion weightings. The diffusion coefficients D are obtained by a linear two-parameter fit according to (*12*)

$$\ln I/I_0 = D\gamma^2 g^2 \delta^2 (\Delta - \delta/3), \qquad [1]$$

where I, γ, g, δ, and Δ refer to the signal intensity, the gyromagnetic ratio, the total gradient strength, the duration of the gradient pulses, and the effective diffusion time, respectively. Although a nonlinear fit with three parameters would take care of the variable diffusion time and T_1 effects, the simple assumption of a single *effective* diffusion time turned out to be fully adequate for a quantitative description of the experimental data. Typically, the evaluation of diffusion coefficients from ROI data yielded correlation coefficients of >0.99 (4–7 gradient strengths).

In cases where the free diffusion of molecules is hindered by boundaries as in biological cells, the *observed* diffusion coefficient becomes dependent on the diffusion time Δ (*12–14*). This particularly holds for the present conditions where a long effective diffusion time of the order of 1 s corresponds to a large displacement of the diffusing spins. In fact, the mean displacement $\bar{x}$ due to diffusion is given by

$$\bar{x} = \sqrt{2D(\Delta - \delta/3)}. \qquad [2]$$

Assuming a diffusion coefficient of 1.0×10^{-5} cm^2 s^{-1} the resulting displacement of about 45 μm is lower than the average cell body of neurons (100 μm) in gray matter, but larger than the typical radii (10–30 μm) of axons with and without myelin sheath as encountered in the bulk of white matter.

EXPERIMENTAL RESULTS

Phantom Studies

The feasibility of diffusion imaging using the modified high-speed STEAM MRI sequence was demonstrated in phantom studies using three tubes filled with polyethylene glycol (PEG), dimethyl sulfoxide (DMSO), and tap water at room temperature. Figure 2 shows single-shot STEAM images acquired with the experimental parameters described above. The duration of the diffusion gradients in both the frequency-encoding and slice selection direction and the effective diffusion time were δ = 8.9 ms and Δ

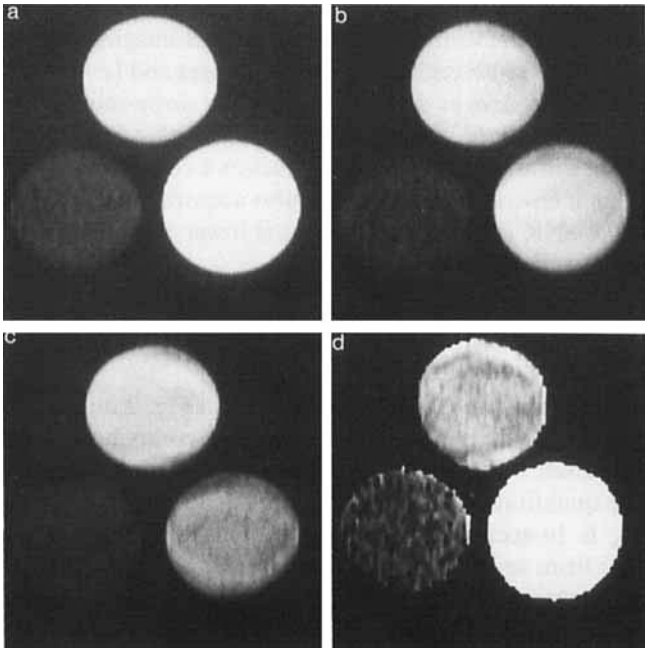

FIG. 2. (a–c) Diffusion-weighted high-speed STEAM images of a phantom consisting of three tubes filled with polyethylene glycol (PEG, lower left), dimethyl sulfoxide (DMSO, top), and tap water (lower right). Diffusion gradients of duration δ = 8.9 ms were applied in both the frequency-encoding and slice selection direction. The total gradient strengths are (a) 1.42, (b) 6.53, and (c) 11.3 mT m^{-1}. A middle interval TM = 760 ms resulted in an effective diffusion time Δ = 1000 ms. The spatial resolution of the images corresponds to a 48 × 128 data matrix covering a 250-mm field-of-view (slice thickness 8 mm). The actual imaging time is 576 ms using n = 48 readout periods of 12-ms duration (α = 12°, TE/2 = 10 ms). The data acquisition interval is 1.92 ms (128 complex data points). (d) Diffusion image calculated from a series of four diffusion-weighted single-shot images (correlation coefficient > 0.9). The brightest intensities correspond to diffusion coefficients $\geq 2.0 \times 10^{-5}$ cm^2 s^{-1}.

= 1000 ms, respectively. Using gradient strengths of (a) 1.0, (b) 4.6, and (c) 8.0 mT m^{-1} in two directions the total applied gradient strength for diffusion weighting was increased by $\sqrt{2}$. The image in Fig. 2d represents a diffusion image calculated from a series of four diffusion-weighted images according to Eq. [1].

Human Brain Studies

Diffusion-weighted high-speed STEAM images of the brain of a normal human volunteer are shown in Fig. 3 with diffusion gradients applied in both the frequency-encoding (horizontal axis in transverse images) and the slice selection direction. While Fig. 3a–3d depict single-shot images without averaging, the data in Fig. 3e–3h represent the average of eight sequentially acquired images from different heartbeats a minimum of 10 s apart. They were acquired to facilitate a more quantitative evaluation of diffusion coefficients by improved SNR. In both sets of images the diffusion contrasts correspond to the application of total gradient strengths that increase from 1.4 mT m^{-1} (left) to 11.3 mT m^{-1} (right). Signal loss in the eyes is due to movements of the vitreous body.

In complete analogy to Fig. 3, the images in Figs. 4 and 5 show transverse EKG-triggered diffusion-weighted images of the brain of normal volunteers at slightly higher levels through and above the ventricles, respectively. All imaging parameters are identical to Fig. 3 with (a–d) representing single-shot images and (e–h) representing eight accumulations for quantitative evaluations. Again, the single-shot images demonstrate the absence of motion-induced phase-encoding artifacts that have been observed with conventional slower diffusion-imaging techniques as a consequence of CSF-mediated brain pulsations. In a few cases, images were also acquired with 16 accumulations to accomodate for the SNR of white matter that is lower than that of the gray matter due to its shorter T_1 relaxation time.

DISCUSSION

Phantom Studies

The experimental results on phantoms as shown in Fig. 2 not only demonstrate a reasonable SNR of single-shot images in cases where the components exhibit sufficiently long T_1 relaxation times, but they also cover an adequate range of accessible diffusion contrasts. A more quantitative evaluation of the data based on ROI pixel intensities is depicted in Fig. 6. In accordance with Eq. [1] the graph shows a semilogarithmic plot of ROI values from seven diffusion-weighted images as a function of the square of the diffusion gradient strength. Solid lines refer to least-squares fits yielding diffusion coefficients of (2.2 ± 0.1), (0.7 ± 0.1), and $(0.5 \pm 0.1) \times 10^{-5}$ cm^2 s^{-1} for water, DMSO, and PEG, respectively. These values are in excellent agreement with previously determined diffusion coefficients using conventional techniques (*4, 15*). The results hold for diffusion imaging experiments with diffusion times of $\Delta \geqslant 1000$ ms. For a diffusion time of 760 ms the calculated diffusion coefficients turned out to be about 10% smaller.

Molecular Self-Diffusion in Human Brain

EKG-triggered high-speed STEAM MRI of the human brain (Figs. 3–5) emerges as a new technique that allows the acquisition of diffusion-weighted images without

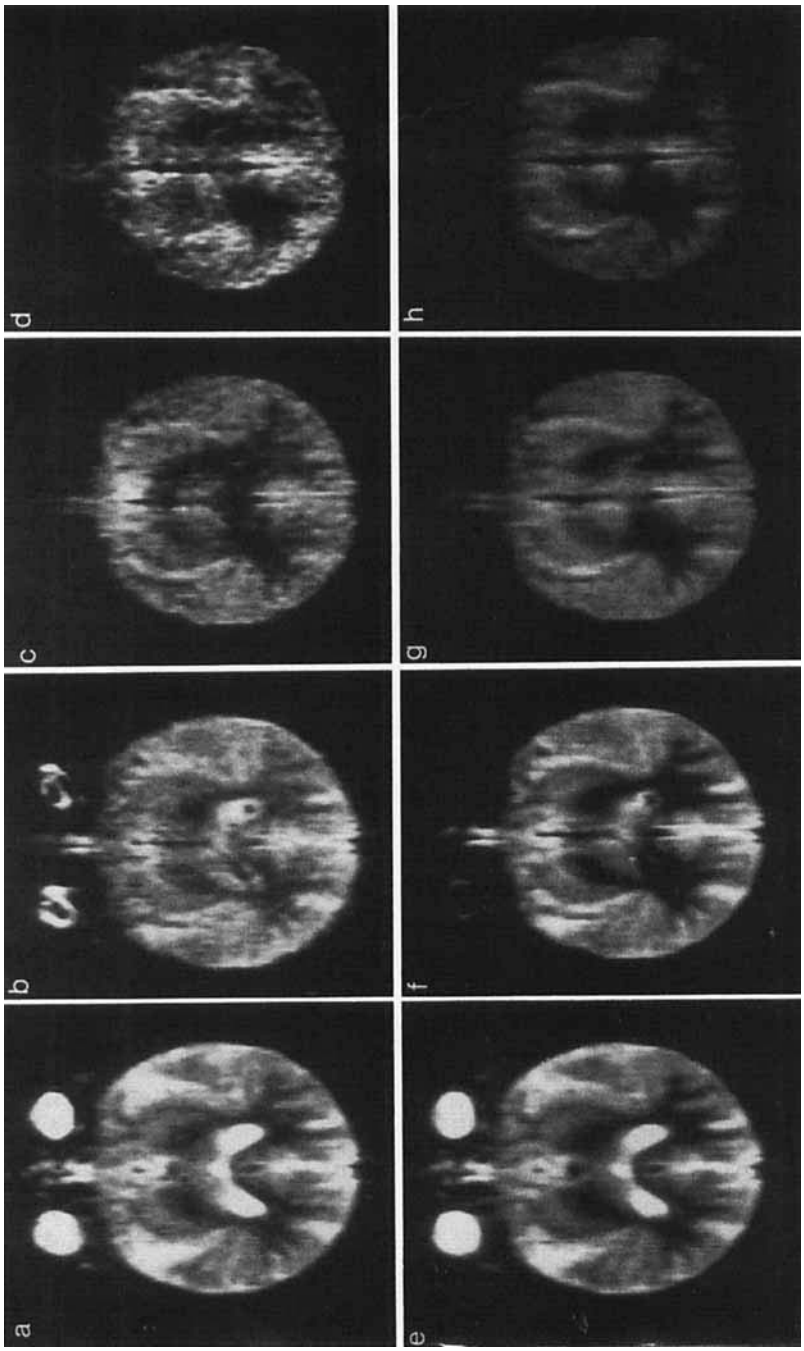

FIG. 3. Transverse EKG-triggered diffusion-weighted high-speed STEAM images of the brain of a normal volunteer at the level of the eyes. The images were acquired using an EKG delay of 300 ms with diffusion gradients in both the frequency-encoding and slice-selection directions increasing from left (1.42 mT m^{-1}) to right (11.3 mT m^{-1}). Other parameters are as in Fig. 2. (a–d) Single-shot images, (e–h) averages from eight accumulations from different heartbeats a minimum of 10 s apart.

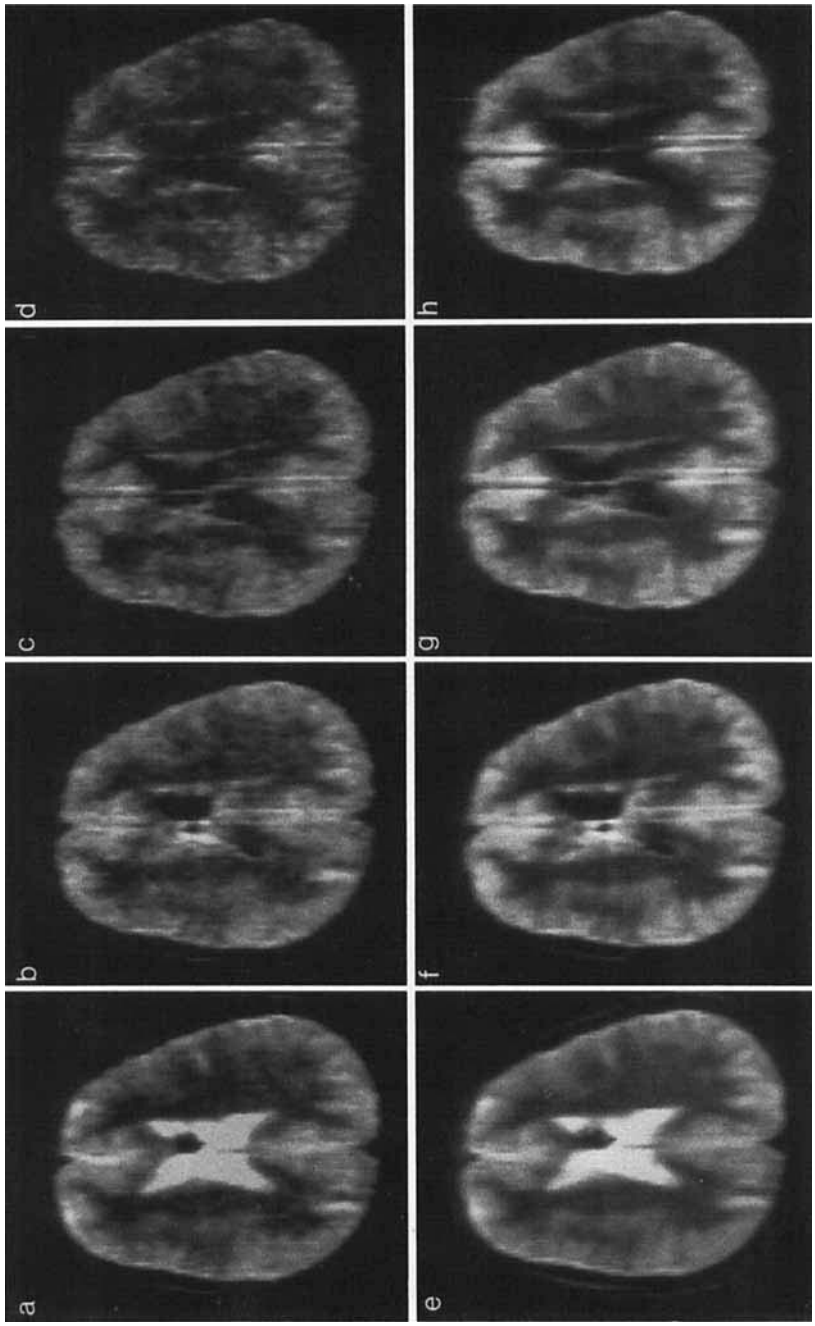

FIG. 4. Transverse EKG-triggered diffusion-weighted high-speed STEAM images of the brain of a normal volunteer at the level of the ventricles. Imaging parameters are as in Fig. 3. (a–d) Single-shot images, (e–h) averages from eight accumulations.

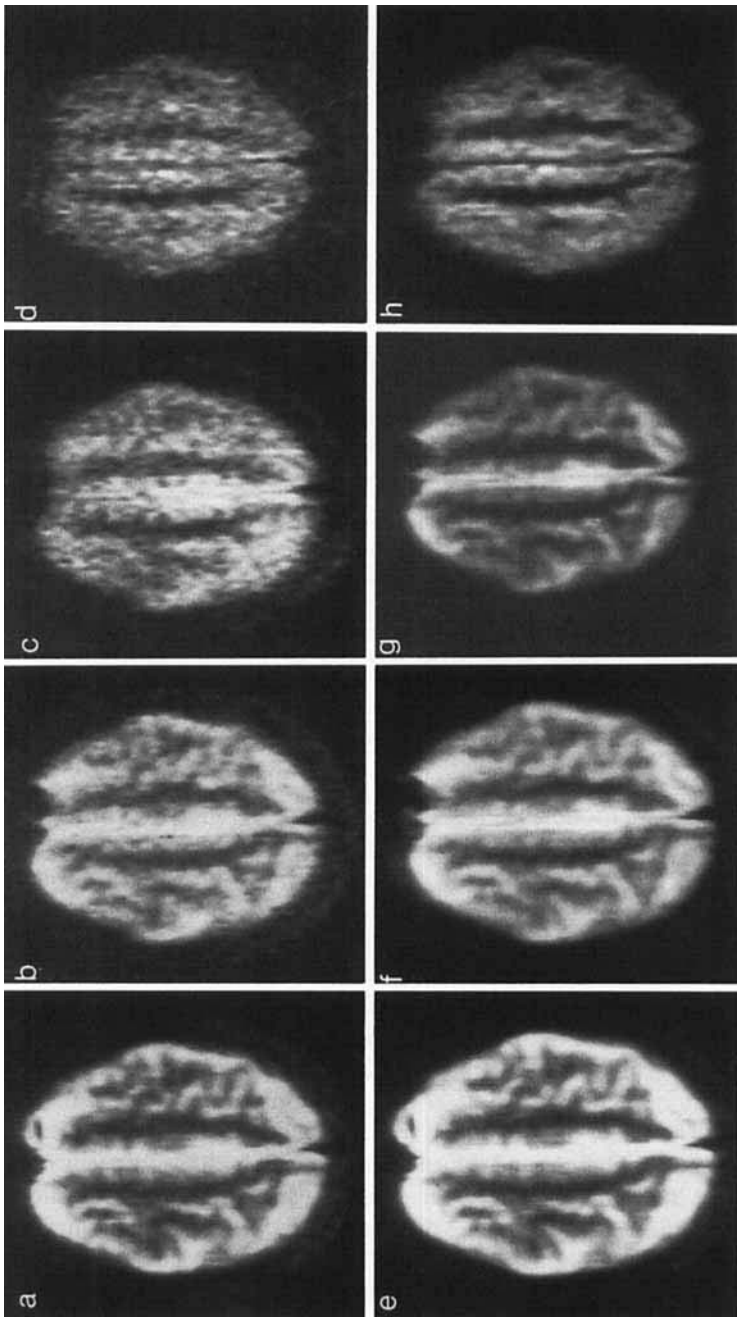

FIG. 5. Transverse EKG-triggered diffusion-weighted high-speed STEAM images of the brain of a normal volunteer at a level above the ventricles. Imaging parameters are as in Fig. 3. (a–d) Single-shot images, (e–h) averages from eight accumulations.

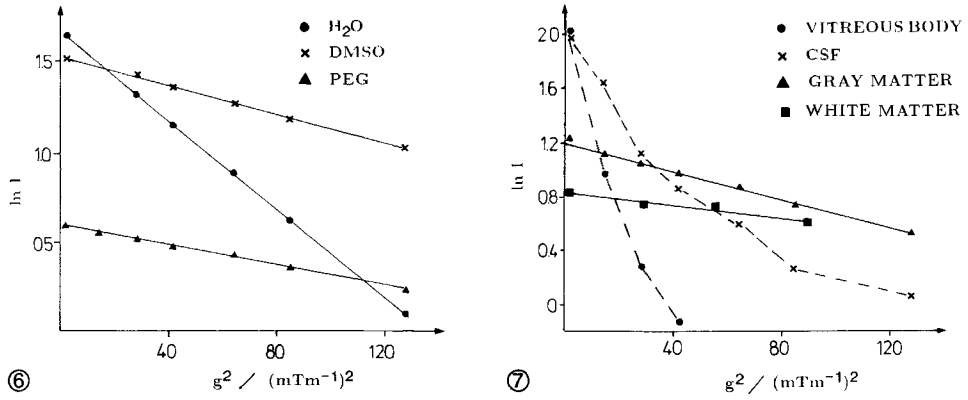

FIG. 6. Semilogarithmic plot of region-of-interest signal intensities from a series of seven diffusion-weighted high-speed STEAM images of the phantom shown in Fig. 2. The data represent single-shot images without averaging. The solid lines correspond to least-squares fits of the data according to Eq. [1] yielding diffusion coefficients of (2.2 ± 0.1), (0.7 ± 0.1), and $(0.5 \pm 0.1) \times 10^{-5}$ cm^2 s^{-1} for water, DMSO, and PEG at room temperature, respectively.

FIG. 7. Semilogarithmic plot of region-of-interest signal intensities from a series of seven EKG-triggered diffusion-weighted high-speed STEAM images of the normal human brain. The data for gray matter, CSF, and vitreous body represent averages from eight accumulations with the simultaneous application of two diffusion gradients at the level of the eyes as shown in Fig. 3. The data for white matter represent averages of 16 accumulations using only one diffusion gradient perpendicular to the myelin sheath of the neurofibrils at a level above the ventricles as shown in Fig. 5. The solid lines correspond to least-squares fits of the data according to Eq. [1] yielding diffusion coefficients of $(1.0 \pm 0.1) \times 10^{-5}$ cm^2 s^{-1} for gray matter and $(0.3 \pm 0.1) \times 10^{-5}$ cm^2 s^{-1} for white matter (perpendicular orientation). The data for both the vitreous body and the CSF (broken lines, no fits) are affected by the presence of macroscopic motion and/or flow.

being compromised by motion artifacts. This finding parallels recent observations with diffusion-weighted EPI of the human brain (*16, 17*). However, while SNR considerations indicate a disadvantage with respect to EPI, major practical advantages result from the fact that the RF refocused STE signals are completely free from signal losses due to susceptibility-induced local magnetic field gradients. This applies particularly to regions where brain tissue is close to air-filled cavities in the head. A typical example is the area between the eyes in the transverse plane shown in Fig. 3 where echo-planar images suffer from an almost complete signal loss over a wide area.

Figure 7 depicts a semilogarithmic plot of ROI values from seven diffusion-weighted images of the brain of a normal volunteer as a function of the square of the diffusion gradient strength. The data were obtained from the same slice as were those in Fig. 3, using eight image accumulations and diffusion gradients in both the frequency-encoding and slice-selective direction. However, the data for white matter were obtained from 16 image accumulations using only one diffusion gradient in the frequency-encoding direction *perpendicular* to the main orientation of the myelin fibers. In all cases the data of four different ROIs were averaged together, since individual evaluations resulted in diffusion coefficients that varied by less than 10%.

The observed signal attenuation for CSF and the vitreous body is entirely attributed to flow and eye movements, respectively. The solid lines in Fig. 7 correspond to least-

squares fits yielding diffusion coefficients of $(1.0 \pm 0.1) \times 10^{-5}$ cm^2 s^{-1} for gray matter and $(0.3 \pm 0.1) \times 10^{-5}$ cm^2 s^{-1} for white matter fibers perpendicular to the diffusion gradient. In general, the experimental data for gray and white matter did not show evidence for a biexponential decay that may be associated with the presence of incoherent microscopic flow (perfusion) (*2*). In fact, the diffusion coefficient for gray matter is identical to that obtained by Kinstry *et al.* (*17*) and close to that of Moseley *et al.* (*18*), while Turner and LeBihan (*19*) reported a 30% lower value assuming a perfusion fraction of about 10%.

Since anisotropy of diffusional processes has been reported for white matter in both cat and human brain (*18–20*) further experiments were carried out to investigate the directional dependence of the diffusion coefficient. For this purpose, the white matter study with only one diffusion-encoding gradient was repeated in the same volunteer with the orientation of the gradient *parallel* to the myelin sheath of the neurofibrils. The position of the transverse slice corresponds to the level shown in Fig. 5. In order to avoid potential complications from a different behavior of the gradients when interchanging the gradient coil functions, the diffusion-weighted STEAM sequence remained unchanged, while the volunteer rotated his head by 90° from an upward position as in Figs. 3–5 to a lying position. As expected the evaluated diffusion coefficient of $(0.5 \pm 0.1) \times 10^{-5}$ cm^2 s^{-1} is higher than $(0.3 \pm 0.1) \times 10^{-5}$ cm^2 s^{-1} obtained for a perpendicular orientation, whereas the diffusion coefficients for gray matter did not show any directional dependence. The fact that the diffusion coefficient parallel to the myelin fibers is higher than in the perpendicular orientation clearly reflects the presence of anisotropic and/or restricted diffusion. For a given diffusion time a higher diffusion coefficient is observed in those directions where the mean displacement of the tissue water molecules is less restricted by the dimensions of the cellular structures.

The present results confirm previous findings about the influence of anisotropic (restricted) diffusion in white matter (*18–20*) and isotropic (unrestricted) diffusion in gray matter as suggested by its larger cell sizes. The low diffusion coefficient for white matter perpendicular to the diffusion encoding is close to that of Ref. (*19*), while values for parallel diffusion gradients were found to be almost twice as high as reported here, i.e. $(1.1 \pm 0.1) \times 10^{-5}$ cm^2 s^{-1} (*17–19*). The discrepancy may be due to a remaining influence of restricted diffusion for the very long diffusion time $\Delta = 1000$ ms used in the high-speed STEAM sequence. This condition is very different from that of diffusion-weighted EPI (and spin-echo) sequences where the short T_2 relaxation times of brain tissue restrict the accessible diffusion times to $\Delta < 100$ ms. For the case of two simultaneously applied diffusion gradients a few studies were performed as a function of diffusion time ranging from 760 to 1480 ms. No significant variation of the diffusion coefficients (ROI data) was observed over this range. However, a more detailed investigation of restricted diffusion is beyond the scope of the present study as well as outside the technical capabilities of the gradient system.

Calculated Diffusion Maps

The anatomical identification of diffusion coefficients may be facilitated by the calculation of diffusion images on a pixel-by-pixel basis and a correlation of these maps to conventional high-resolution MR images. This is demonstrated in Fig. 8

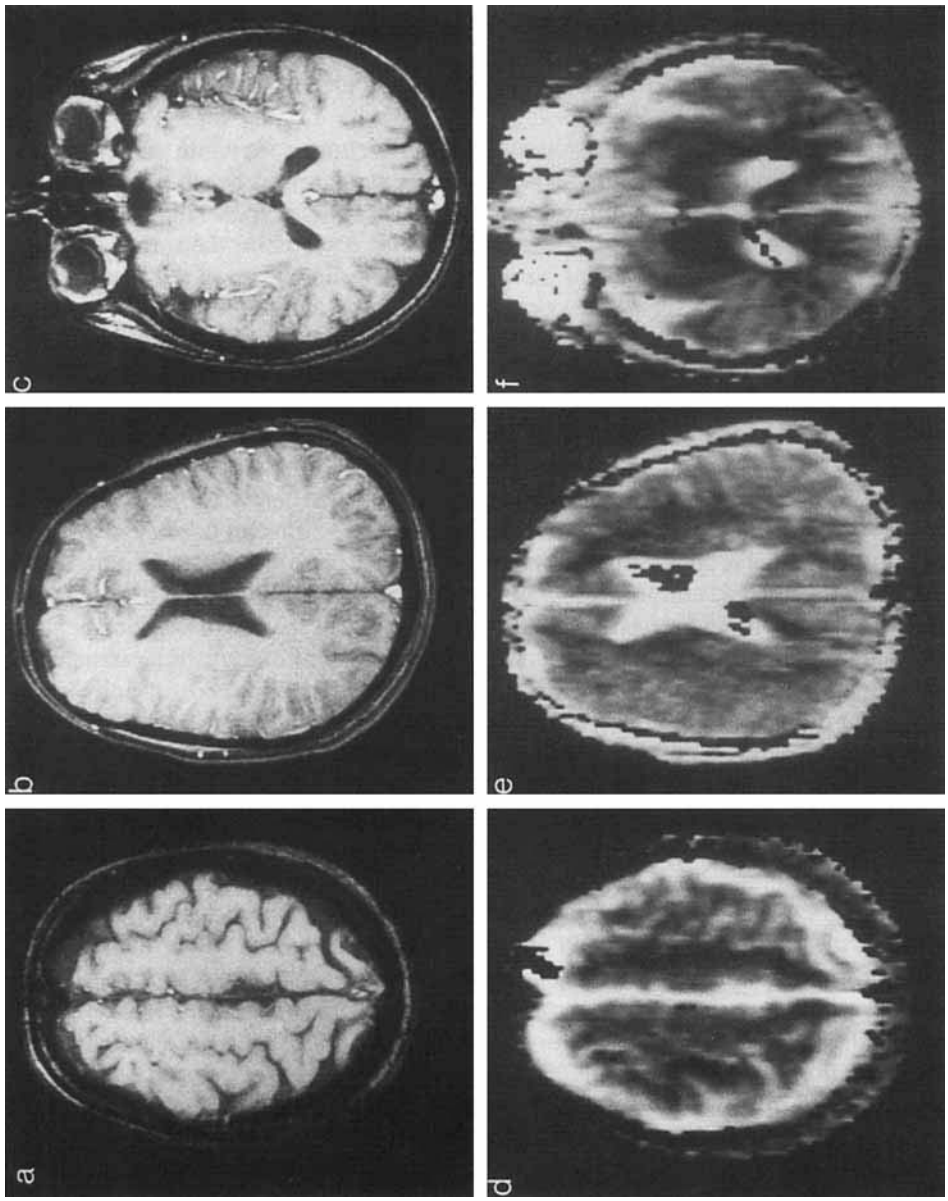
c
f
b
e
a
d

where images (a–c) show conventional T_1-weighted multislice FLASH images of three selected transverse sections of the brain of a normal volunteer. The images (d–f) depict the corresponding diffusion maps calculated from four different diffusion-weighted high-speed STEAM images each using the data averaged from eight single-shot images. Obviously, the SNR of the data per pixel is somewhat lower than that of the ROI values from multiple pixels or even multiple ROIs as used in Fig. 7 for a more accurate determination of diffusion coefficients.

Black pixels in the calculated diffusion maps in Fig. 8 originate from either an unacceptable low signal below a certain threshold or from least-squares fits with a correlation factor ≤ 0.9. When using single-shot images without averaging, it is still possible to obtain similar diffusion images at the expense of almost twice as many black spots. Nevertheless, the possibility of actually calculating such images demonstrates the stability of the high-speed STEAM approach and provides additional confidence and reliability for the given numbers.

CONCLUDING REMARKS

This paper describes a new high-speed STEAM MRI sequence for the acquisition of diffusion-weighted images. Single-shot images with variable degrees of diffusion contrast may be used either directly for qualitative diagnostic purposes, or for a calculation of spatially resolved molecular self-diffusion coefficients. Phantom studies demonstrate the feasibility of quantitative determinations. Residual motion artifacts in studies of human brain *in vivo* are eliminated by EKG triggering. For a diffusion time of $\Delta = 1000$ ms the calculated diffusion coefficients for white matter exhibit a directional dependence that indicates the influence of restricted diffusional processes. Gray matter values are at least twice as high and remain unaffected by orientational changes.

Diffusion-weighted images were obtained within acquisition times of about half a second on a conventional whole-body MRI system equipped with 10 mT m^{-1} gradients. Practical advantages of the high-speed STEAM technique result from the fact that the images behave like conventional spin-echo images, and therefore do not suffer from susceptibility-induced signal losses as observed with echo-planar imaging. A potential disadvantage may be the lower SNR as compared to echo-planar imaging and a restriction to tissues with long T_1 relaxation times as long as gradient strengths are limited to 10 mT m^{-1}. Obviously, these problems are overcome by stronger gradients reducing both the readout period and the TM interval of the single-shot STEAM sequence. In such cases, diffusion-weighted high-speed STEAM images may not only regain SNR and access to short T_1 components but further allow a detailed study of restricted diffusion over a large range of diffusion times.

FIG. 8. (a–c) Transverse FLASH MR images (TR = 100 ms, TE = 6 ms, flip angle 70°, slice thickness 4 mm, field-of-view 250 mm, matrix size 256 × 256) and (d–f) corresponding calculated diffusion maps at three different levels of the human brain as shown in Figs. 3–5. Diffusion coefficients were calculated on a pixel-by-pixel basis from a series of four diffusion-weighted high-speed STEAM images using eight accumulations. Calculated values are only displayed for a correlation coefficient > 0.9. The brightest intensities correspond to diffusion coefficients $\geq 2.0 \times 10^{-5}$ cm^2 s^{-1}.

ACKNOWLEDGMENT

Financial support by the Bundesminister für Forschung und Technologie (BMFT) of the Federal Republic of Germany (Grant 01 VF 8606/6) is gratefully acknowledged.

REFERENCES

1. E. O. STEJSKAL AND J. E. TANNER, *J. Chem. Phys.* **42,** 288 (1965).
2. D. LEBIHAN, E. BRETON, D. LALLEMAND, P. GRENIER, E. CABANIS, AND M. LAVAL-JEANTET, *Radiology* **161,** 401 (1986).
3. P. M. PATTANY, J. J. PHILLIPS, L. C. CHIU, J. L. DUERK, J. M. MCNALLY, AND S. N. MOHAPATRA, *J. Comput. Assist. Tomogr.* **11,** 369 (1987).
4. K.-D. MERBOLDT, H. BRUHN, J. FRAHM, M. L. GYNGELL, W. HÄNICKE, AND M. DEIMLING, *Magn. Reson. Med.* **9,** 423 (1989).
5. D. LEBIHAN, R. TURNER, AND J. R. MACFALL, *Magn. Reson. Med.* **10,** 324 (1989).
6. K.-D. MERBOLDT, W. HÄNICKE, M. L. GYNGELL, J. FRAHM, AND H. BRUHN, *Magn. Reson. Med.* **12,** 198 (1989).
7. K.-D. MERBOLDT, W. HÄNICKE, M. L. GYNGELL, J. FRAHM, AND H. BRUHN, *Magn. Reson. Med.* **82,** 115 (1989).
8. R. TURNER AND D. LEBIHAN, *J. Magn. Reson.* **86,** 445 (1990).
9. J. FRAHM, A. HAASE, D. MATTHAEI, K.-D. MERBOLDT, AND W. HÄNICKE, *J. Magn. Reson.* **65,** 130 (1985).
10. J. FRAHM, W. HÄNICKE, H. BRUHN, M. L. GYNGELL, AND K.-D. MERBOLDT, *Magn. Reson. Med.* **22,** 133–142 (1991).
11. K.-D. MERBOLDT, W. HÄNICKE, AND J. FRAHM, *J. Magn. Reson.* **64,** 479 (1985).
12. J. E. TANNER, *J. Chem. Phys.* **52,** 2523 (1970); *J. Chem. Phys.* **57,** 3586 (1972).
13. E. O. STEJSKAL, *J. Chem. Phys.* **43,** 3597 (1965).
14. R. C. WAYNE AND R. M. COTTS, *Phys. Rev.* **151,** 264 (1966).
15. C. B. AHN, S. Y. LEE, O. NALCIOGLU, AND Z. H. CHO, *Med. Phys.* **13,** 789 (1986).
16. R. TURNER, R. VAVREK, J. MAIER, AND D. LEBIHAN, *in* "Book of Abstracts, Society of Magnetic Resonance in Medicine, Berkeley, WIP," p. 1123, 1989.
17. R. C. MCKINSTRY, R. M. WEISSKOFF, M. S. COHEN, J. M. VEVEA, K. K. KWONG, R. R. RZEDZIAN, T. J. BRADY, AND B. R. ROSEN, *in* "Book of Abstracts, Society of Magnetic Resonance Imaging, 8th Annual Meeting, WIP," p. 5, 1990.
18. M. E. MOSELEY, Y. COHEN, J. MINTOROVITCH, L. CHILEUITT, H. SHIMIZU, J. KUCHARCZYK, M. F. WENDLAND, AND P. R. WEINSTEIN, *Magn. Reson. Med.* **14,** 330 (1990).
19. R. TURNER, D. LEBIHAN, AND A. S. CHESNICK, *Magn. Reson. Med.* **19,** 247 (1991).
20. M. E. MOSELEY, J. KUCHARCZYK, H. S. ASGARI, AND D. NORMAN, *Magn. Reson. Med.* **19,** 321 (1991).